From film to ring: quasi-circular inorganic lead halide perovskite grain induced growth of uniform lead silicate glass ring structure

Guoqing Tong,[1] Wentao Song,[1,2] Luis K. Ono[1] and Yabing Qi[1, a)]

AFFILIATIONS

[1]Energy Materials and Surface Sciences Unit (EMSSU), Okinawa Institute of Science and Technology Graduate University (OIST), 1919-1 Tancha, Onna-son, Kunigami-gun, Okinawa, 904-0495, Japan.

[2]Department of Physics and Atmospheric Science, Sir James Dunn Building, 6310 Coburg Road Dalhousie University, Halifax, Nova Scotia, Canada, B3H 4R2.

[a)]Author to whom correspondence should be addressed: Yabing.Qi@OIST.jp

G. Tong and W. Song contributed equally to this work.

ABSTRACT: Polycrystalline properties of perovskites can induce the growth of different nanostructures thanks to their facile fabrication. In this work, the $CsPb_2Br_5$ perovskite grains were used as templates to induce the growth of the ring-like structures on a SiO_2/Si substrate. Owing to the oxidation of the volatile $PbBr_2$ originated from the decomposition of $CsPb_2Br_5$, the grain boundaries of perovskites are prone to reaction with SiO_2, which leads to the formation of Pb-silicate glass at high temperatures. The quasi-circular grain structure of $CsPb_2Br_5$ defines the final dimension of the Pb-silicate glass ring-like structures. XPS measurement results reveal the formation and composition of Pb-silicate glass ring-like structures converting from the halide

perovskite film on the SiO_2/Si substrate. Furthermore, these ring-like structures can extend to the field of display and pulsed-laser by combining existing techniques.

Microstructures such as nanowires (NWs) and microwires (MWs), and quantum dots have been intensively studied for their distinctive properties and prospective applications.[1-5] Different from nano/microstructures with a solid interior, nano-ring (NR)/micro-ring (MR) possess a unique hollow space, which allows greater tunability through additional degrees of freedom (i.e., inner and outer ring diameters).[6, 7] A wide variety of applications based on NR/MR have already emerged. For example, III–V semiconductor MR arrays[8] and $CsPbBr_3$ perovskite MR arrays[9] have shown lasing capability as miniature lasers. Si MRs[10] and $MAPbBr_3$ MRs[11] could be used as optical resonators and next-generation color printing.[12] Moreover, gold nano-rings are widely used in various fields such as light-matter interaction and plasmonic sensing applications owning to their localized surface plasmon resonance properties.[13, 14] Tremendous efforts have been devoted to improving the quality of nanoring structures and finding a facile technique to boost their yield. For example, nanosphere lithography[9, 15, 16], electron beam lithography[17, 18] and self-assembly growth[19-21] are used to produce nanoring structures, however, low precision in nanoring dimension control or complex process and expensive cost makes them far more challenging in large scale fabrication.[13, 22]

Halide perovskites are receiving increasing academic/commercial interest due to their outstanding optoelectronic properties and high efficiency in solar cells and LEDs.[23-25] Currently, many researchers are focusing on the improvement of efficiency and device lifetime. However, halide perovskites also have other excellent physical and chemical properties, which can be utilized for nano/micro-structure fabrication. For

example, the facile and controllable synthesis of perovskites can be used to construct different nano/micro-structures such as thin film,[26, 27] NW/MW arrays,[28-31] quantum dots,[32, 33] and nanorings,[9, 21] and applied in photodetectors, LEDs and lasers. Different from the lead halide perovskites, lead-bearing silicate glass (PbO-SiO_2) has an extremely long human use history.[34] The excellent properties of lead-bearing silicate glass make it one of the key materials in the field of materials science, chemistry, and physics.[35] For example, lead silicate glass have been studied as radiation shielding glass[36] and as coating of thermoelectric materials.[37] Their H_2-reduced form is currently the most used glass material for micro-channel plates in electron multipliers.[38-40]

Herein, we report the Pb-silicate glass ring structures with a micrometer scale diameter by employing the lead halide perovskite as both the precursor and template. The quasi-circular grain structure of $CsPb_2Br_5$ perovskite in the annealing procedure shows uniform grain size and serves as the template to induce the formation of ring-like structure. Additionally, the continuous decomposition of $CsPb_2Br_5$ also provides sufficient $PbBr_2$ to be oxidized in ambient, which readily reacts with SiO_2 layer of the SiO_2/Si substrate to form Pb-silicate glass confirmed by XPS results. Following the decomposition of perovskites and oxidation of volatile $PbBr_2$, the evenly distributed ring structures were formed. DI-H_2O washing and acid leaching on these ring structures and the corresponding chemical composition change monitored by XPS further confirmed lead silicate is the component of the ring-like structures. This work provides us a facile method to fabricate high quality and mass-produced lead silicate glass MR structures for advanced applications.

Figure 1 illustrates the formation of ring-like structures. Firstly, a $CsPb_2Br_5$ perovskite film of one micrometer thickness was deposited on the SiO_2/Si substrates by vapor deposition (Figure S1). Then the as-prepared samples were placed on the hotplate (400 ^oC) and annealed at 700 ^oC for 60 min under air. After cooling down to the room temperature, the as-formed ring-like structures were obtained. It is found that the ring-like structures are evenly distributed on the substrates as seen in Figure 2a and S2. The measured diameters on one of the ring-like structures are 11.45, 11.25 and 11.75 μm, respectively (Figure 2b), suggesting this structure is very close to a circle. Statistical analyses of 73 rings (Figure S3) give an average ring diameter of 25 $\pm$ 8 μm. Atomic force microscopy (AFM) measurements were further conducted to evaluate the morphology and structure of the ring-like structure. As seen in Figures 2c-d and S4, there is significant height variation of the ring-like structure edge, which may result from the different decomposition rate of the perovskite grains, further leading to the different growth rate of ring-like structure edge.

Firstly, the EDS element map of as-formed ring-like structure (Figure S5) exhibits that the ring is composed mainly of Pb element, but also it contains Si, O and Cs elements. Interestingly, Br does not show significant signal intensity on the ring edges compared to Cs, suggesting there is significant amount of Cs concentrated on the ring structure edges versus insignificant amount of Br. Moreover, the *ex-situ* XPS was used to reveal the surface composition of the ring-like structure. The peak location and intensity are very consistent across all 3 sampling positions (Figure S6), suggesting high uniformity of the surface composition. All the presented peaks were assigned in Figure S7 ("As-formed").

The narrow scans have been further performed on the as-formed rings on SiO_2/Si substrate for quantification and chemical state analysis. The O 1s, Pb 4f, Si 2p, Br 3d, Cs 3d and C 1s XPS narrow scan results are shown in Figures 3 and S8 ("as-formed"), respectively. The most distinctive feature in Figure 3a is the splitting of the O 1s signal, which shows two superimposed peaks at binding energy (B.E.) and full-width-half-

maximum (FWHM) (in brackets) of 531.9 eV (1.5 eV) and 530.2 eV (1.3 eV) with separation in peaks (ΔB.E.) of 1.7 eV. These values demonstrate remarkable agreement with previous XPS studies on Pb-silicate glass material system ($R_2O{\cdot}PbO{\cdot}SiO_2$, R is alkaline/alkaline earth metal and could be absent) with O 1s at 531.7 eV (1.38 eV) and 530.1 eV (1.40 eV) with ΔB.E. of 1.6 eV,[41-44] and at 532.2 eV and 530.3 eV with ΔB.E. of 1.9 eV.[45] On the basis of these studies, the higher binding energy of O 1s peak at 531.7 – 532.2 eV originates from the Si-O-Si bridging oxygen (BO) in the Si-O-Si-O network of the Pb-silicate glass, while the lower binding energy of O 1s peak at 530.1 – 530.3 eV is caused by the modification of Si-O-Si-O network by Pb to form non-bridging (NBO) Pb-O-Si and probably Pb-O-Pb. This interpretation of O 1s signal is further confirmed by the Pb 4f (Figure 3b) and Si 2p (Figure 3c) signals. The Pb $4f_{5/2}$ peak position at 143.2 eV (1.4 eV) and Pb $4f_{7/2}$ peak position at 138.4 eV (1.4 eV) are extremely consistent with the literature XPS result of Pb^{2+} in lead silicate glass at Pb $4f_{5/2}$ – 143.3 eV (1.33 eV) and Pb $4f_{7/2}$ – 138.4 eV (1.33 eV).[41-44] The Si 2p signal shows a single peak at binding energy 102.2 eV (1.9 eV), within range of the Si in the silicate anion of Pb-silicate glass literature result at 101.6 eV (1.85 eV) – 102.6 eV.[41-45] The percentage atomic concentration ratio of Pb:Si:O determined by the peak areas is 10.2%:18.7%:52.2% (Table S1).

The Br and Cs are also identified on the surface. The Br 3d region shows two spin-orbit splitting peaks at binding energies of 69.2 eV (Br $3d_{3/2}$) and 68.1 eV (Br $3d_{5/2}$) (Figure S8b), in excellent agreement with both $CsPbBr_3$ (Br $3d_{5/2}$ 68.1 eV)[46] and CsBr (Br $3d_{5/2}$ 68.1 eV).[47] However, the annealing temperature of the $CsPbBr_3$ to form the ring-like structure at ~700 °C surpasses the decomposition temperature of $CsPbBr_3$ at ~350 °C,[31, 48] while the CsBr has much higher thermal stability (660 °C).[31, 49] The Br 3d peaks are therefore unequivocally attributed to CsBr. The Cs 3d signal exhibits two spin-orbit splitting peaks at Cs $3d_{3/2}$–738.3 eV (1.6 eV) and Cs $3d_{5/2}$ – 724.3 eV (1.6 eV) (Figure S8c), in agreement with the previous XPS work of CsBr at Cs $3d_{3/2}$ – 738.3 eV and Cs $3d_{5/2}$ – 724.3 eV.[50] The percentage atomic concentration of Cs and Br is only 2.8% and 1.3%, an order of magnitude lower than that of Pb (10.2%), Si (18.7%), and

O (52.2%). The location of the Cs^+ cation in the Pb-silicate glass atomic structure is worth further discussion. The presence of alkaline and alkaline earth metal ions is frequent in the Pb-silicate glass material system. Previous XPS study on Pb-silicate glass containing Cs displays Cs $3d_{5/2}$ peak position at 724.5 eV,[50] only 0.2 eV different from our Cs $3d_{5/2}$ result. It is likely that the extra Cs^+ ions diffuse into the host structure of the $PbO{\cdot}SiO_2$ glass, possibly leading to the formation NBO Cs-O-Si at atomic level.

It is well known that the Pb-silicate is insoluble in H_2O.[51] A previous study showed that acids could be used to leach out Pb and alkaline metal from Pb-silicate glass in aqueous solution, whereas CsBr readily dissolves in H_2O.[45] To further understand the chemical composition of these ring-like structures on Si, the as-formed sample was treated with deionized (DI) water and concentrated HCl. Firstly, the as-formed sample was dried with compressed N_2 gas after being washed thoroughly with DI H_2O. The dried sample was next checked by optical microscope and transferred into the EDS and XPS system for composition and surface analysis, respectively. The surface morphology under optical microscope remains the same as the as-formed sample (Figure S9). The EDS map of ring-like structure shows Pb, Si, O, Cs elements in Figure S10, which is close to the as-formed sample (Figure S5). Similarly, the XPS spectra in Figure S11 are consistent across different positions and one representative spectrum is shown in Figure S7 ("DI H_2O washed"). The O 1s, Pb 4f, Si 2p, Br 3d, Cs 3d and C 1s spectra of the same surface are shown in Figures 3 and S8, respectively.

The XPS results of the DI H_2O washed sample show the peaks of Cs 3d, O 1s, C 1s, Pb 4f, Si 2p, and Br 3d. Further quantification based on the narrow scan results showed the chemical identity of these species remain unchanged after the DI H_2O washing. The percentage atomic concentration (Table S1) showed Pb, Si and O remaining as the dominant species on the DI-H_2O washed sample while the amounts of Cs and Br were reduced by half. This result is consistent with the low H_2O solubility of the Pb-silicate glass and high H_2O solubility of CsBr. The remaining Cs and Br amounts identified on the washed sample are likely inside the bulk of the Pb-silicate glass and thus inaccessible to the H_2O during washing.

The as-formed Pb-silicate glass ring-like structure was next tested against acid in aqueous environment. The as-formed sample was immersed in a beaker filled with concentrated HCl overnight and the corresponding optical microscope image is shown in Figure S12. Different from the other two cases, the Pb element in the HCl-leached sample is absent as seen in EDS map (Figure S13). The XPS spectra of the HCl-leached sample show high consistency across 3 different positions (Figure S14), and one representative spectrum is shown in Figure S7 titled "HCl leached". Cs, Br, and Pb signals previously observed on the as-formed and DI H_2O washed samples have disappeared on the surface. Only 3 elements – Si, O, and C have been found. The narrow scan spectra comparison in Figures 3 and S8 further confirmed the complete removal of Pb, Br, and Cs by concentrated HCl leaching. The removal of Pb and Cs also eliminates all NBO (Pb-O-Si, and possibly Cs-O-Si, and Pb-O-Pb), thus converts Pb-bonded O to BO (Si-O-Si). Indeed, the O 1s spectra in Figure 3a only shows a single peak, in sharp contrast to the two-peak splitting feature (530.2 eV for NBO, and 531.9-532.1 eV for BO) typical of Pb-silicate glass in the as-formed and DI-H_2O washed samples. The O 1s single peak position also shifted to higher binding energy of 533.1 eV. Consistent with O 1s evolution after HCl leaching, the Si 2p overall signal also shifted from 102.2-102.4 eV typical of the Pb-silicate glass to higher binding energy at 103.7 eV, very close to the binding energy of Si-O-Si bond in SiO_4 tetrahedron in SiO_2 at 103.5 eV. The peak evolution of both O 1s and Si 2p are in excellent agreement with previous XPS result on the leaching of Pb-silicate glasses in acid under aqueous environment.[45]

To further understand the evolution and verify the peak deconvolution of the Si 2p and O 1s XPS signal after the HCl leaching, we performed XPS on pristine Si where SiO_2 is the dominant species on the surface (Figures S15 and S16) and compared the Si 2p and O 1s signal with that of the HCl-leached sample (Figure 3). The Si 2p signal comparison between Figures 3c and S16a confirmed the deconvolved Si 2p peak at 103.7 eV (1.4 eV) is from SiO_2. The much smaller deconvolved Si 2p peak at 102.2 eV (1.3 eV) is attributed to Si-OH formed by ionic exchange reaction taking place during

HCl leaching (Scheme 1).[45] The O 1s signal comparison between Figures 3a and S16b confirmed the deconvolved O 1s peak at 532.9 eV (1.2 eV) is from SiO_2. The much larger deconvolved O 1s peak at 533.2 eV (1.6 eV) is attributed to silanol Si-OH based on Scheme 1. The convolved O 1s peak positions and FWHM are consistent with literature.[52, 53]

$$\equiv Si\text{-}O\text{-}Pb\text{-}O\text{-}Si\equiv + 2H^{+} \rightarrow 2\equiv Si\text{-}OH \text{ (silanol)} + Pb^{2+} \qquad \text{Scheme 1}$$

The disappearance of Cs and Br with the dissolution of the Pb-silicate glass by concentrated HCl is worth a detailed discussion. We have showed the reduced amount of Cs and Br identified by XPS in the DI-H_2O washed sample. Since CsBr is soluble in H_2O, the CsBr exposed during H_2O washing have been removed. But the H_2O-insoluble Pb-silicate glass protects the CsBr inside the bulk of Pb-silicate from being exposed. Chemical testing using concentrated HCl dissolved the Pb-silicate glass structure and exposed all CsBr inside the structure, leading to its concurrent dissolution in the concentrated HCl.

To further understand the quasi-circular grain induced the growth of the ring-like structures, we first investigated their formation process. The $CsPb_2Br_5$ deposited by thermal evaporation shows uniform and full coverage film with small grain size (Figure 4 and Figure 1 step ①). These small grains will fuse into large grains aiming to reduce the surface energy under continuous heating (400 °C, step ②). According to the Ostwald ripening mechanism, these small grains will continuously grow until they disappear. These enlarged grains would serve as templates to create the ring-like structures. In brief, the dimension of these enlarged grains will determine the final diameter of the ring-like structures. In parallel, the continuous increase of the annealing temperature accelerates the decomposition of these perovskite grains. It is well known that the deposition of perovskites usually starts from the grain boundaries.[31, 54, 55] This decomposition process can be explained as follows:[31, 49]

$$CsPb_2Br_5 \rightarrow CsPbBr_3 + PbBr_2 \uparrow$$

$$CsPbBr_3 \rightarrow CsBr + PbBr_2 \uparrow$$

To clearly observe this growth procedure, one of the representative grains was chosen as object of research. During this air annealing process, the $PbBr_2$ will rapidly transform into liquid state and vaporize due to the low melting temperature of $PbBr_2$ (357 °C).[56] It is worth noting that the gaseous state of $PbBr_2$ will be substantially oxidized to PbO ($PbBr_2 + ½\ O_2 \rightarrow PbO + Br_2$).[57] More importantly, the oxidized PbO is prone to react with SiO_2 to construct silicate glass at a high temperature. The product of silicate glass will serve as an outline to impede the grain growth. As the annealing temperature increases to 700 °C, the inner grain will start to decompose (Figure 1-step ④-⑤). The CsBr has a high melting point around 660 °C.[31] Prolong the annealing time at 700 °C to 20 min and 40 min leads to the gradual disappearance of inner grains because of the volatilization of CsBr and $PbBr_2$ (Figure 1-step ⑤). After one-hour annealing, the ring-like structure is obtained (700 °C/60 min, Figure 1-step ⑥). Benefiting from this quasi-circular grain induced growth, high yield of the ring-like structures as well as the joint ring-like structures were obtained (Figure S17).

As a comparison, the same annealing process was conducted under nitrogen environment. It is found that the isolated structures are of poor quality (Figure S18). This can be attributed to the absence of oxygen that makes volatile $PbBr_2$ difficult to transform to PbO, which impedes the reaction between PbO and SiO_2 layer to form the Pb-silicate rings. Additionally, pure $PbBr_2$ film was made by depositing 700 nm thickness of $PbBr_2$ on the SiO_2/Si substrates via vapor deposition method. The same annealing procedure was performed in the ambient environment. In this case, the final products on the substrates are the large grains instead of well distribution ring-like structures (Figure S19). Based on above analysis, these large grains would be PbO or $PbBr_2$ covered with thicker layer of PbO, which makes them difficult to evaporate because of the high melting point of PbO (889 °C).[58] To identify this hypothesis, EDS mapping were performed to investigate the component of these large grains. As seen in Figures S20-S21, large amounts of lead within the large grains in the EDS line scan indicates the major component is PbO. In addition, the same procedures were conducted in air by using FTO and Si substrates. It is worth to note that no rings are observed on

the FTO substrate (Figures S22), and the rings grown on the Si substrate are porous (Figures S23, more detail can be found in Supporting information). These experiments further corroborate the mechanism proposed on ring-like structure growth.

In conclusion, we have prepared the lead silicate glass ring-like structure on SiO_2/Si substrates by using the inorganic lead halide perovskite $CsPb_2Br_5$ film as a precursor. The approximate round grain structure of $CsPb_2Br_5$ and the oxidation of $PbBr_2$ from the decomposition of $CsPb_2Br_5$ at high temperature annealing allow the chemical reaction with SiO_2 to form the Pb-silicate glass based ring-like structures. The as-prepared ring-like structures on Si surface showed the signature of Cs, Br, Pb, Si, and O based on the XPS measurement results, which further confirms the composition of Pb-silicate glass based rings on the SiO_2/Si substrates. This finding offers a breakthrough for nanoring structures in mass production and is expected to pave an avenue for halide perovskite materials.

See the supplementary material for more details on experimental procedures and other information.

This work was supported by funding from the Energy Materials and Surface Sciences Unit of the Okinawa Institute of Science and Technology Graduate University, the OIST Proof of Concept (POC) Program, and the OIST R&D Cluster Research Program. We thank the OIST Micro/Nanofabrication Section and Imaging Section for the support.

AUTHOR DECLARATIONS

Conflict of Interest

We state that we have no conflicts of interest to disclose.

DATA AVAILABILITY

The data that support the findings of this study are available from the corresponding authors upon reasonable request.

REFERENCES

[1]Y. Shu; X. Lin; H. Qin; Z. Hu; Y. Jin; X Peng, Angew.Chem. Int. Ed. 59, 22312 (2020).

[2]Q. Lin, S. Bernardi, B. Shabbir, Q. Ou, M. Wang, W. Yin, S. Liu, A. S. R. Chesman, S. O. Fürer, G. Si, N. Medhekar, J. Jasieniak, A. Widmer-Cooper, W. Mao, U. Bach, Adv. Funct. Mater. 2021, DOI: 10.1002/adfm.202109442.

[3]Z. Wang, T. Yang, Y. Zhang, Q. Ou, H. Lin, Q. Zhang, H. Chen, H. Y. Hoh, B. Jia, Q. Bao, Adv. Mater. 32, 2001388 (2020).

[4]Z. Dai, Q. Ou, C. Wang, G. Si, B. Shabbir, C. Zheng, Z. Wang, Y. Zhang, Y. Huang, Y. Dong, J. J. Jasieniak, B. Su, Q. Bao, J. Mater. Chem. C 7, 5954 (2019).

[5]C. Zhou, G. Cao, Z. Gan, Q. Ou, W. Chen, Q. Bao, B. Jia, X. Wen, ACS Appl. Mater. Interfaces 11, 26017, (2019).

[6]T. H. Chow; Y. Lai; X. Cui; W. Lu; X. Zhuo; J. Wang, *Small* 15, 1902608, (2019).

[7]M. Sun; N. Kreis; K. Chen; X. Fu; S. Guo; H. Wang, *Chem. Mater*. 33, 8546 (2021) .

[8]W. W. Wong; Z. Su; N. Wang; C. Jagadish; H. H. Tan, *Nano Lett*. 21, 5681, (2021).

[9]J. Xu, S. Xu, Z. Qi, C. Wang, C. Lu, Y. Cui, Nanoscale **10**, 10383 (2018).

[10]W.-C. Hsu, C. Zhen, A. X. Wang, ACS Photonics **8**, 1933 (2021).

[11]S. X. Li, H. Xia, G. P. Zhang, X. L. Xu, Y. Yang, G. Wang, H. B. Sun, Adv. Mater. Technol. **5**, 2000051 (2020).

[12]X. Liu, Z. Huang, J. Zang, Nano Lett. **20**, 8739 (2020).

[13]S. Mu, H. Chen, C. Shi, J. Zhang, B. Yang, Nano Research **14**, 4674 (2021).

[14]C. Y. Tsai, J. W. Lin, C. Y. Wu, P. T. Lin, T. W. Lu, P. T. Lee, Nano Lett. **12**, 1648 (2012).

[15]M. Bayati, P. Patoka, M. Giersig, E. R. Savinova, Langmuir **26**, 3549 (2010).

[16]R. M. C. Aaron R. Halpern, ACS Nano **7**, 1755 (2013).

[17]R. Near, C. Tabor, J. Duan, R. Pachter, M. El-Sayed, Nano Lett. **12**, 2158 (2012).

[18]M. Lorente-Crespo, L. Wang, R. Ortuno, C. Garcia-Meca, Y. Ekinci, A. Martinez, Nano Lett. **13**, 2654 (2013).

[19]L. W. Yu, K. J. Chen, J. Song, J. Xu, W. Li, X. F. Li, J. M. Wang, X. F. Huang, Phys. Rev. Lett. **98**, 166102 (2007).

[20]W. L. Hughes, Z. L. Wang, Appl. Phys. Lett. **86**, 043106 (2005).

[21]Y. Zheng, T. Yang, Z. Fang, M. Shang, Z. Zhang, J. Yang, J. Fan, W. Yang, X. Hou, T. Wu, Nano Research **13**, 2994 (2020).

[22]W. Liu, J. Wang, X. Xu, C. Zhao, X. Xu, P. S. Weiss, ACS Nano **15**, 12180 (2021).

[23]G. Tong, L. K. Ono, Y. Liu, H. Zhang, T. Bu, Y. B. Qi, Nano-Micro Lett. **13**, 155 (2021).

[24]N. F. Jamaludin, B. Febriansyah, Y. F. Ng, N. Yantara, M. Li, D. Giovanni, J. Fu, Y. B. Tay, T. B., T. C. Sum, N. Mathews, and S. Mhaisalkar, Appl. Phys. Lett. **119**, 154101 (2021).

[25]M. H. Wong, Q. An, J. Kress, J.-M. Morsdorf, J. Ballmann, and Y. Vaynzof, Appl. Phys. Lett. **119**, 233903 (2021).

[26]G. Tong, D.-Y. S., L. K. Ono, Y. Liu, Y. Hu, H. Zhang, A. Jamshaid, L. Qiu, Z. Liu, Y. B. Qi. Adv. Energy Mater. **11**, 2003712 (2021).

[27]T. Chen, G. Tong, E. Xu, H. Li , P. Li, Z. Zhu, J. Tang, Y. B. Qi, Y. Jiang, J. Mater. Chem. A **7**, 20597 (2019).

[28]W. Deng, L. Huang, X. Xu, X. Zhang, X. Jin, S. T. Lee, J. Jie, Nano Lett. **17**, 2482 (2017).

[29]L. Gao, K. Zeng, J. Guo, C. Ge, J. Du, Y. Zhao, C. Chen, H. Deng, Y. He, H. Song, G. Niu, J. Tang, Nano Lett. **16**, 7446 (2016).

[30]G. Tong, M. Jiang, D.-Y. Son, L. Qiu, Z. Liu, L. K. Ono, Y. B. Qi, ACS Appl. Mater. Interfaces **12**, 14185 (2020).

[31]G. Tong, M. Jiang, D. Y. Son, L. K. Ono, Y. B. Qi, Adv. Funct. Mater. **30**, 2002526 (2020).

[32]N. Wang, L. Cheng, R. Ge, S. Zhang, Y. Miao, W. Zou, C. Yi, Y. Sun, Y. Cao, R. Yang, Y. Wei, Q. Guo, Y. Ke, M. Yu, Y. Jin, Y. Liu, Q. Ding, D. Di, L. Yang, G. Xing, H. Tian, C. Jin, F. Gao, R. H. Friend, J. Wang, W. Huang, Nat. Photonics **10**, 699 (2016).

[33]J. Li, L. Xu, T. Wang, J. Song, J. Chen, J. Xue, Y. Dong, B. Cai, Q. Shan, B. Han, H. Zeng, Adv. Mater. **29**, 1603885 (2017).

[34]R. J. CHARLESTON, Archaeometry 1960.

[35]H. I. Kim, S. Lee, E. J. Kim, S. K. Lee, J Am Ceram Soc. **104**, 1318 (2020).

[36]S. Ruengsri, Sci. Technol. Nucl. Install. **2014**, 1 (2014).

[37]D. B.-A. a. Y. G. Yatir Sadia, J. Mater. Res. **34**, 3563 (2019).

[38]J. Jia, Y. Zhang, X. Zhang, Y. Sun, Y. Wang, L. Zhang, J. Liu, C. Wang, H. Yu, IOP Conf. Ser.: Mater. Sci. Eng. **612**, 032109 (2019).

[39]J. Jia, Y. Zhang, Y. Sun, X. Zhang, Y. Wang, L. Zhang, J. Liu, C. Wang, Z. Fan, IOP Conf. Ser.: Mater. Sci. Eng. **612**, 032110 (2019).

[40]Y. Zhang, Y. Sun, J. Wang, K. Huang, Y. Wang, J. Liu, J. Jia, B. Zhang, W. Hou, X. Lv, IOP Conf. Ser.: Mater. Sci. Eng. **423**, 012167 (2018).

[41]K. N. Dalby, H. W. Nesbitt, V. P. Zakaznova-Herzog, P. L. King, Geochim. Cosmochim. Acta **71**, 4297 (2007).

[42]D. H. I.A. Gee, C.F. McConville, Phys. Chem. Glasses 41, 339 (2001).

[43]T. P. A. L. B.M.J.Smets, J. Non-Crystalline Solids **48**, 423 (1982).

[44]J. Zemek, P. Jiricek, J. Houdkova, K. Jurek, O. Gedeon, J. Non-Crystalline Solids **469**, 1 (2017).

[45]R. Bertoncello, L. Milanese, A. Bouquillon, J. C. Dran, B. Mille, J. Salomon, Appl. Phys. A **79**, 193 (2004).

[46]Q.-B. Yan, N. Bao, S.-N. Ding, J. Mater. Chem. B **7**, 4153 (2019).

[47]Z. Li, J. Xu, S. Zhou, B. Zhang, X. Liu, S. Dai, J. Yao, ACS Appl. Mater. Interfaces **10**, 38183 (2018).

[48]H. Li, G. Tong, T. Chen, H. Zhu, G. Li, Y. Chang, L. Wang, Y. Jiang J. Mater. Chem. A **6**, 14255 (2018).

[49]G. Tong, L. K. Ono, Y. B. Qi, Energy Technol. **8**, 1900961 (2020).

[50]S. N. T. Hatta, Y. Manpuku, N. Matsumoto, H. Yamada, Hyomen Kagaku 44, (2013).

[51]K. Funasaka, T. Tojo, S. Kaneco, M. Takaoka, Atmos. Pollut. Res. **4**, 362 (2013).

[52]H. B. D.Sprenger, W.Meisel, P.Gütlich, J. Non-Crystalline Solids **126**, 111 (1990).

[53]D. L. A. Gary W.Simmons, KamilKlier, J. Electron Spectrosc. **105**, 197 (1999).

[54]J. S. Yun, J. Kim, T. Young, R. J. Patterson, D. Kim, J. Seidel, S. Lim, M. A. Green, S. Huang, A. Ho-Baillie, Adv. Funct. Mater. **28**, 1705363 (2018).

[55]Z. Liu, L. Qiu, E. J. Juarez-Perez, Z. Hawash, T. Kim, Y. Jiang, Z. Wu, S. R. Raga, L. K. Ono, S. F. Liu, Y. B. Qi, Nat. Commun. **9**, 3880 (2018).

[56]G. Tong, T. Chen, H. Li, L. Qiu, Z. Liu, Y. Dang, W. Song, L. K.Ono, Y. Jiang, Y. B. Qi, Nano Energy **65**, 104015 (2019).

[57]J. L. Hyde, J Am Ceram Soc. **73**, 1860 (1951).

[58]J.-H. Ji, D.-J. Shin, J. Kim, J.-H. Koh, Ceram. Int. **46**, 4104 (2020).

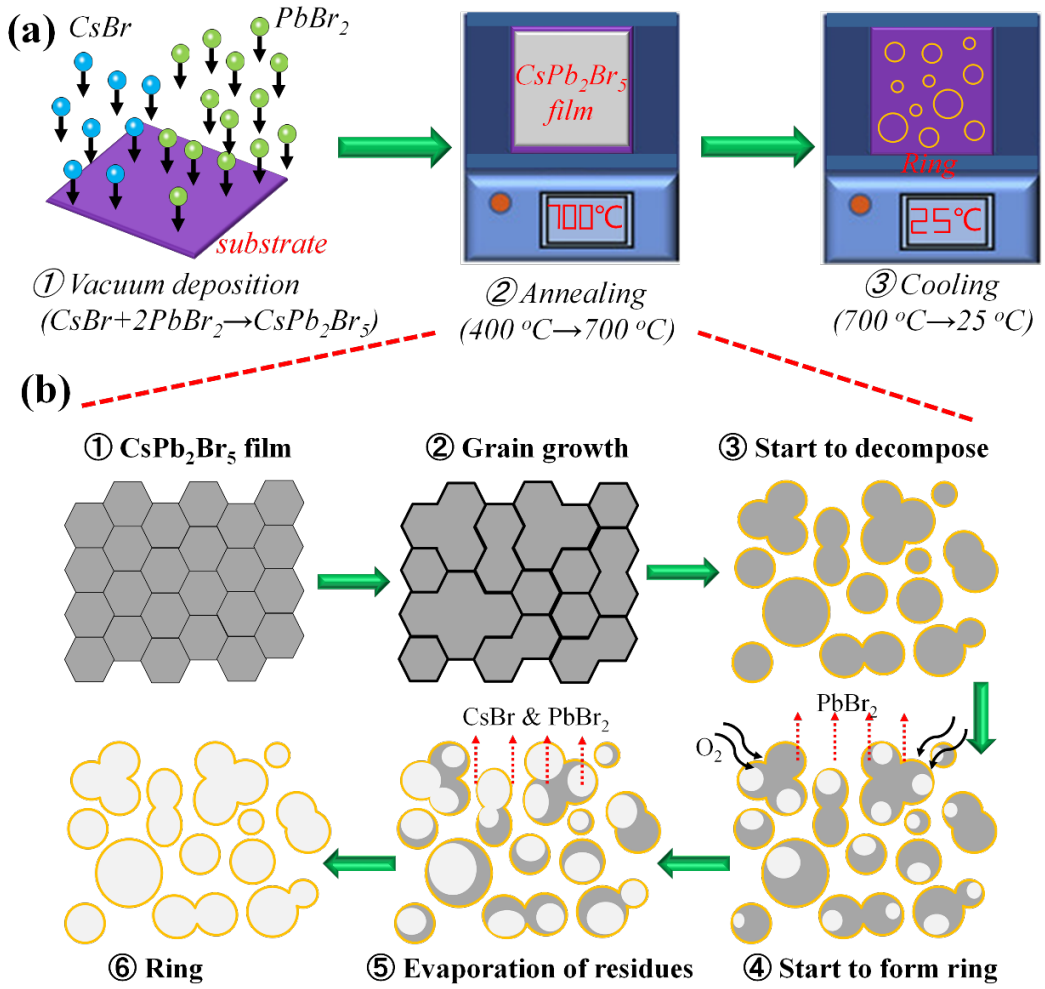

FIG. 1. (a) Schematic illustration of formation of ring-like structures and (b) the formation of ring-like structures.

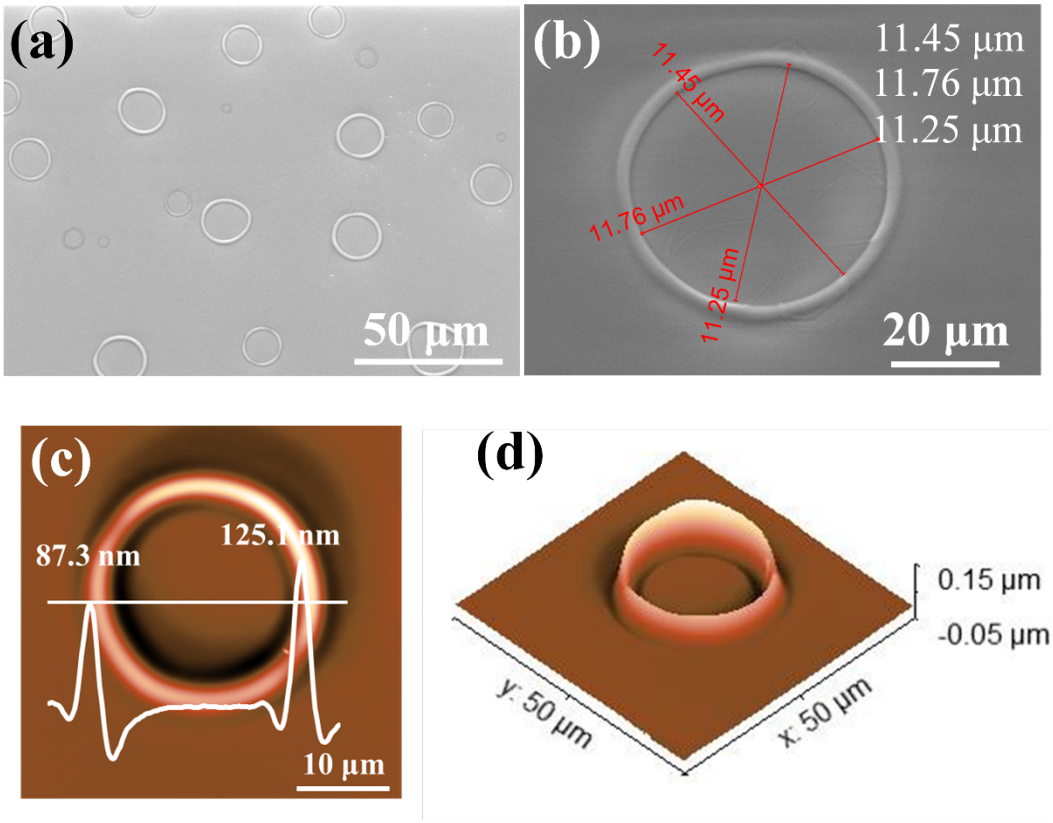

FIG. 2. (a) Low and (b) high magnification scanning electron microscope (SEM) images of the ring-like structures; (c, d) Atomic force microscopy (AFM) morphology images of the single ring-like structure.

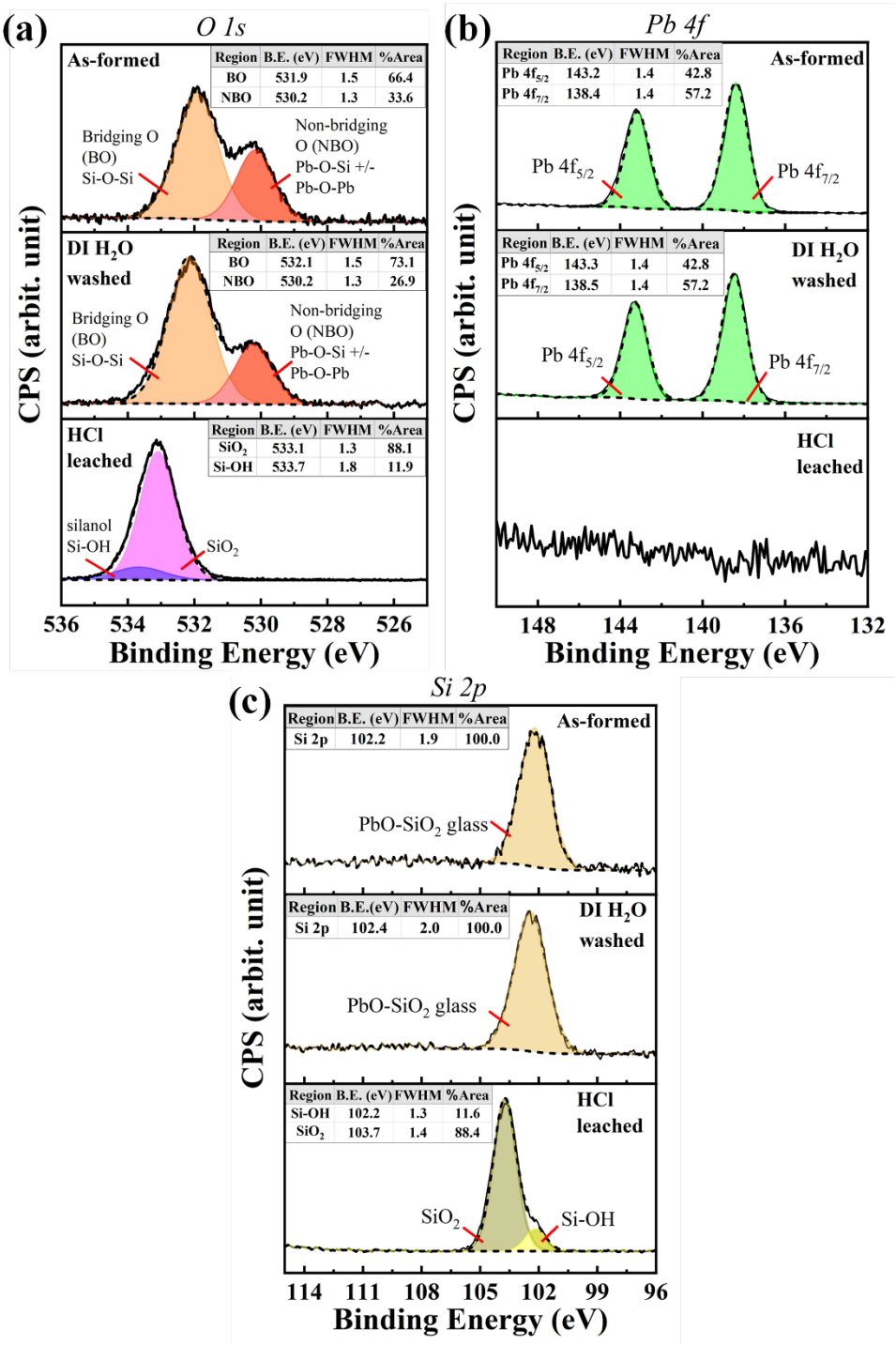

FIG. 3. XPS narrow scans of as-formed (upper panel), DI-H_2O washed (middle panel), HCl-leached (lower panel) ring-like structures on SiO_2/Si substrates in the region of (a) O 1s, (b) Pb 4f and (c) Si 2p.

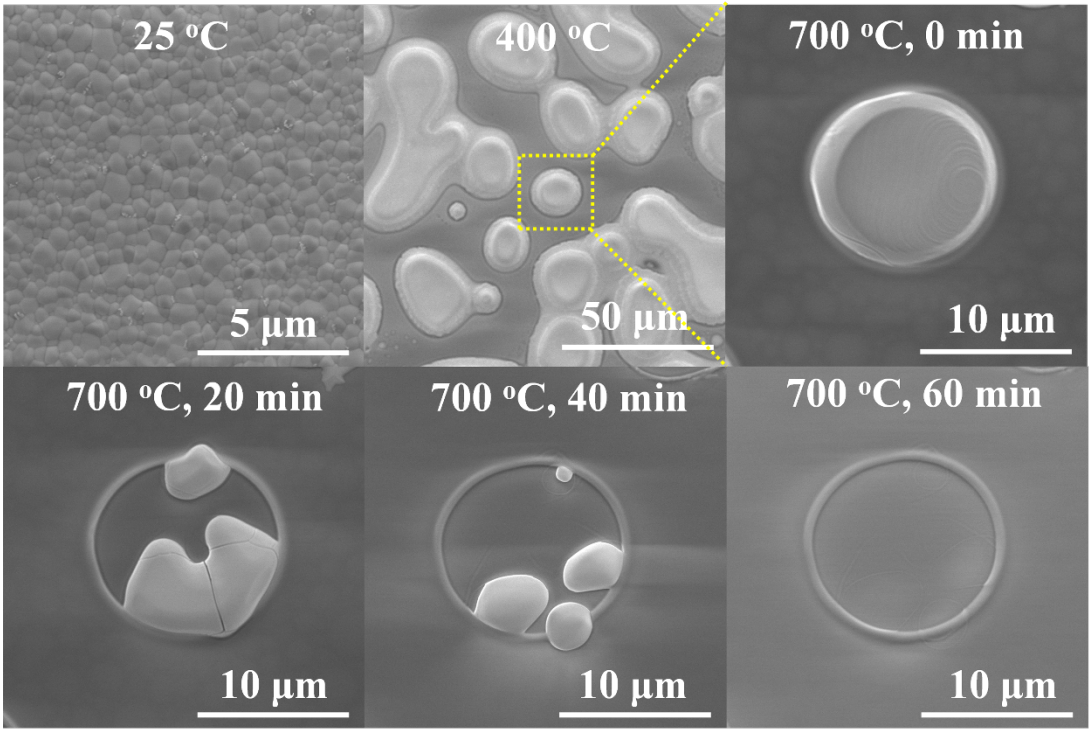

FIG. 4. SEM images of the conversion process of the $CsPb_2Br_5$ precursor film to the ring-like structures under different conditions.